Journal of Engineering Mathematics **31:** 411–437, 1997.

Solidification of aluminium spray-formed billets

Heat flow in the bulk deposit

I.A. FRIGAARD*
Abteilung für Industriemathematik, Johannes-Kepler-Universität, Linz, Austria

Received 1 June 1995; accepted in revised form 21 May 1996

Abstract. Transient heat transfer and solidification within an axisymmetric spray-formed aluminium billet are investigated. The boundary of the solid billet grows outwards, due to deposition from a stream of atomised semi-solid metal droplets. Within the billet, it is necessary to determine the heat fluxes and, in particular, to determine the position of the solidus isotherm. Mathematically, one must solve a nonlinear two-dimensional parabolic initial-boundary-value problem in an irregular and expanding domain.

The problem is formulated within the general framework of billet heat transfer. An effective numerical algorithm is developed and implemented. Results from the numerical algorithm are used to explore thermal transients in the start-up phase of billet spray-forming production runs, the phenomenem of steady-state heat flow in the billet crown and the complex dependence of heat flow on billet-surface movement.

Key words: Spray-forming, solidification, heat transfer, computation, moving-boundary problems

1. Spray-forming

Cylindrical aluminium-alloy billets of over 1 m in length and with a diameter $\approx$300 mm may be produced by the spray-forming process, taking 20–30 minutes to grow. The process involves atomisation of liquid metal into a spray of droplets which is propelled rapidly towards a rotating cylindrical collector. The billet grows on top of the collector through the intermittent deposition of thin layers of alloy. As the billet grows, it is withdrawn slowly away from the spray. As well as billets, spray-forming of tubes, thin discs and metal strip are possible; see [1, 2, 3] for reviews of spray-forming technology and applications.

Solidification of the metal takes place within the spray, [4, 5, 6, 7, 8], as well as following deposition, [9, 10, 11, 12, 13]. Typically, a metal layer of thickness $\sim$ 1 mm, corresponding to $\sim 10^2$ layers of flattened droplets, will be deposited in a pulse lasting $\sim 10^{-1}$s. Billet-growth rates are typically $\sim$ 1 mm/s; thus, deposition is intermittent. Microstructural features such as microsegregation, interstitial porosity formation, gas entrapment and grain-size determination, are believed to be largely determined by heat fluxes close beneath the billet surface, during and directly after deposition, [14, 15]. Recent studies have used computational fluid-dynamics techniques to model the impingement of (1 or 2) semi-solid metal droplets on a surface, [16, 17, 18]. Deposition/spreading times are $\sim 10^{-6} - 10^{-5}$s, thermal equilibrium typically takes $\sim 10^{-4}$s. The discrete droplet approach therefore provides excellent insight into microscopic features of deposition, (*e.g.* contact, spreading, micropore formation), but is less able to give insight into sub-surface heat flow that is driven by thin semi-solid layering. In [19], a continuum model was developed to investigate heat fluxes close beneath the surface during deposition. The boundary-layer approach adopted in [19] is complementary to both the discrete droplet

* Present address: Schlumberger Cambridge Research, High Cross, Madingley Road, Cambridge, CB3 0EL, United Kingdom

studies [16, 17, 18] and to this paper, which considers solidification of the entire billet of its growth.

Not all microstructural features of importance are determined by the transient boundary-layer heat fluxes or on the droplet scale. For example, macrosegregation requires that there is a significant liquid fraction, persisting within a geometrically significant portion of the billet over a reasonably long timescale, (*i.e.* minutes). Secondly, thermal shrinkage defects may occur on the microscopic scale or over a much larger length-scale, due to macroscopically non-uniform heat flows. As an example, between the billet and the collector, a significant amount of shrinkage always occurs, since the first spray which impacts is rapidly chilled by the collector. Such thermo-physical processes, and the resulting defects, are best understood through study of solidification on length- and timescales which are appropriate to the billet size.[1] This provides the first motivation for this paper. A second motivation for the paper is that modelling provides the simplest way to understand billet solidification. Billet production takes place in an inert atmosphere within a sealed chamber. Billet rotation and clouds of recirculating metal spray make accurate robust on-line measurement of billet temperature nearly impossible.

Mathematically, the modelling of bulk billet solidification results in a non-trivial moving-boundary problem. The first moving boundary is the billet surface. The second moving boundary of interest is the solidus isotherm within the billet. Billet surface growth has been studied extensively and the dynamics are now reasonably well understood; (see [19] for thin layering, see [20, 21, 22, 23] for time-averaged growth dynamics of the bulk billet; see [24] for growing optimally shaped billets; see [25] for on-line control of billet shape). Billet solidification on a slow timescale and over a large length-scale has not been studied much, [13, 20]. The problem is a two- or three-dimensional nonlinear parabolic initial-boundary-value problem, which must be solved in an irregular expanding domain.

An outline of the paper is as follows. In Section 2, the dimensionless equations governing billet solidification on the billet length-scale and over a slow (billet-growth) timescale are introduced and their relationship to the boundary-layer equations is discussed. Section 3 outlines significant features of the computational algorithm for solution of the slow-time heat-flow problem and presents test computations to demonstrate its robustness and reliability. In Section 4 a number of practical process situations are modelled to gain insight into how to better control macroscopic heat flows in the billet spray-forming process. The paper concludes with a brief discussion. Throughout, a hat (*i.e.*$\hat{}$) is used to denote a dimensional quantity and bold typeface denotes a vector quantity.

2. Billet solidification

Heat transfer within a solidifying aluminium billet manufactured via the spray-forming process is modelled by the following dimensionless initial-boundary-value problem, derived in [19, 20]

$$\frac{\partial H}{\partial t} = \frac{\epsilon}{Pe}\,\boldsymbol{\nabla}\cdot[D(H)\boldsymbol{\nabla}H], \qquad \mathbf{x}\in\Omega(t), \tag{1}$$

$$-D(H)\,\frac{\partial H}{\partial n} = B_{\text{gas}}(T(H)-T_{\text{gas}}) + \frac{Pe}{\epsilon}\,v_{\mathbf{x}_P}(H-H_{\text{spray}}), \quad \mathbf{x}\in\partial\Omega(t): z>0, \tag{2}$$

$$D(H)\,\frac{\partial H}{\partial z} = B_{\text{collector}}(T(H)-T_{\text{collector}}), \qquad \mathbf{x}\in\partial\Omega(t): z=0, \tag{3}$$

$$H(\mathbf{x},t_0) = H_0(\mathbf{x}), \qquad \mathbf{x}\in\Omega(t_0). \tag{4}$$

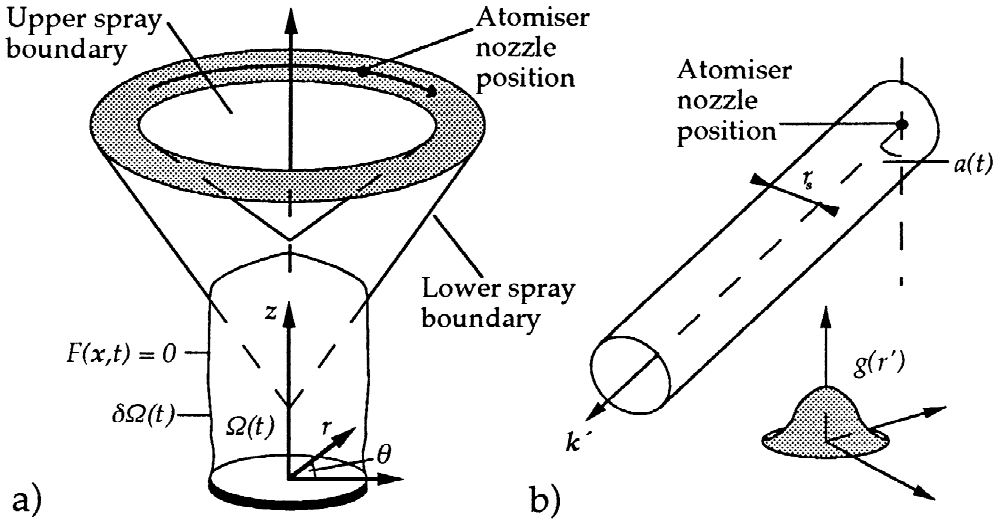

Figure 1. Spray-forming geometry: a) billet coordinates, b) spray coordinates.

The model assumes that heat transfer is conduction-dominated. The main physical justifications for this are: (i) that significant cooling of the spray droplets occurs before impact with the surface, (ii) that the deposited layers of spray are thin, not usually permitting the accumulation of a significant liquid fraction, and (iii) that cooling of the billet surface by the atomising gas is a reasonably effective means of extracting the remaining heat of fusion. Where the spray-formed deposit is quite thin and is held stationary, not all of these conditions need apply, (*e.g.* continuous spraying of a thin metal strip), but in the case of billet spray-forming these conditions are almost essential for successful production.

The billet forms on the top of a rapidly rotating circular collector plate which is positioned to intercept the semi-solid metal spray. Coordinates $\mathbf{x}$ are fixed to the top of the collector plate and rotate with the billet and collector. The z-coordinate is chosen to point vertically upwards. The billet volume at time t is denoted by $\Omega(t)$ and its boundary by $\partial\Omega(t)$, (see Figure 1).

The main dependent variable in (1)–(4) is the enthalpy of the alloy, $H(\mathbf{x}, t)$; $D(H)$ and $T(H)$ denote the diffusivity and temperature functions, respectively. Other variables which appear in (1)–(4) are the temperature of the atomising gas close to the billet surface, T_{gas}, the normal surface velocity, $v_{\mathbf{x}_P}$, the enthalpy of the semi-solid metal spray at the point of deposition, H_{spray}, and the collector temperature, $T_{\text{collector}}$. Initial conditions $H_0(\mathbf{x})$ are prescribed at time $t = t_0 \geq 0$.

The variables in (1)–(4) have been made dimensionless by the scaling of all lengths with the billet radius $\hat{R}$, time with the period of rotation of the billet $2\pi/\hat{\omega}$, and the enthalpy, diffusivity and temperature functions as follows:

$$H = \frac{\hat{H} - \hat{H}_s}{\hat{\rho}\hat{c}\Delta\hat{T}}, \qquad D(H) = \frac{\hat{\rho}\hat{c}}{\hat{K}_s}\,\hat{D}(\hat{H}), \qquad T(H) = \frac{\hat{T}(\hat{H}) - \hat{T}_s}{\Delta\hat{T}}. \tag{5}$$

In (5), the solidus and liquidus temperatures, freezing range, solidus enthalpy, liquid and solid-phase thermal conductivity, density and specific heat capacity, are denoted by $\hat{T}_s, \hat{T}_l, \Delta\hat{T}, \hat{H}_s$, $\hat{K}_l, \hat{K}_s, \hat{\rho}$ and $\hat{c}$, respectively. The latter three quantities are evaluated at a temperature close to the solidus temperature of the alloy.

2.1. DIMENSIONLESS GROUPS

The dimensionless groups in (1)–(4) and their typical sizes are

$$\epsilon \equiv \frac{2\pi \hat{U}_0}{\hat{\omega}_0 \hat{R}} \ll 1, \tag{6}$$

$$Pe \equiv \frac{\hat{\rho}\hat{c}\hat{U}_0\hat{R}}{\hat{K}_s} = O_S(1), \tag{7}$$

$$B_{\text{gas}} = \frac{\hat{h}_{\text{gas}}\hat{R}}{\hat{K}_s} = O_S(1), \tag{8}$$

$$B_{\text{collector}} = \frac{\hat{h}_{\text{collector}}\hat{R}}{\hat{K}_s} = O_S(1), \tag{9}$$

where $O_S(1)$ means that the variables are numerically of size 1. The small parameter ϵ denotes the ratio of the rotation timescale to the withdrawal timescale. The Peclet number *Pe* is the ratio of the timescales for conduction, (or solidification), and that for billet growth; $\hat{U}_0$ denotes a typical speed at which the collector/billet is being withdrawn vertically downwards. The two Biot numbers B_{gas} and $B_{\text{collector}}$ model the heat losses to the gas and collector, respectively. The parameters $\hat{h}_{\text{gas}}$ and $\hat{h}_{\text{collector}}$ denote heat transfer coefficients. Although B_{gas} is included here as a dimensionless group, it should be understood that $\hat{h}_{\text{gas}}$, (and hence B_{gas} also), will vary significantly with position on the billet surface.

2.2. BILLET SURFACE MOVEMENT

Properly considered, the model (1)–(4) is three-dimensional. In terms of coordinates $(\mathbf{x}, t)$ the surface $\partial\Omega(t)$ may be described by an equation $F(\mathbf{x}, t) = 0$ and the surface normal velocity $v_{\mathbf{x}_P}$ is then given by

$$v_{\mathbf{x}_P} = -\frac{\partial F}{\partial t}|\boldsymbol{\nabla} F|^{-1}.$$

The following dimensionless evolution equation for $F(\mathbf{x}, t)$ is derived in [20, 21].

$$\frac{1}{\epsilon}\frac{\partial F}{\partial t}(\mathbf{x}, t) = [\gamma(\dot{m}g\mathbf{k}', F)\dot{m}(t)g(r'[\mathbf{x}, t])\mathbf{k}'(t).\boldsymbol{\nabla}]F(\mathbf{x}, t), \quad \mathbf{x} \in \partial\Omega(t). \tag{10}$$

In (10) γ is a simplified shadowing coefficient, which takes values 0 and 1 according to whether or not the billet surface is shadowed from the spray. The mass flow rate through the atomiser is denoted $\dot{m}(t)$. The coordinate r' measures distance perpendicular to the spray cone axis, and $\mathbf{k}'$ denotes the unit vector in the direction of the spray cone axis at time t, (see Figure 1b). Spray is distributed only within a radius r_s of the spray-cone axis. The mass-flux distribution within the spray cone is described by the positive function $g(r')$. These terms are explained further in [20, 21].

2.2.1. *Slow-time heat flow*

Although (1)–(4) and (10) are three-dimensional, spray-formed billets are nearly always observed to be axisymmetric, with respect to the z-axis. Three-dimensional asymmetry is

usually confined to very thin layers of alloy, (of thickness $O(\epsilon)$), deposited on top of the billet. During a production run, the rotation of the billet and the oscillation of the spray tend to "average out" the asymmetric deposition. If only billet growth is considered, then the averaging procedure may be treated more formally, (see [20, 21]). For a wide class of practically relevant billet shapes, it is possible to demonstrate that the time-averaged equations for billet growth provide an $o(\epsilon)$ asymptotic approximation to the solution of (10), which remains valid for a time period $\eta = O_S(1)$. Here η denotes the "slow-time" variable

$$\eta = \epsilon t. \tag{11}$$

If synchronization of the spray oscillation and the rotation is avoided, the time-averaged equations are axisymmetric and the order of approximation is likely to remain $O(\epsilon)$ throughout the process run, (see [20, 21]).

Motivated by the validity and practical utility of the axisymmetric time-averaged billet growth equations, the following time-averaged version of (1)–(4) is considered for the remainder of this paper.

$$\frac{\partial H}{\partial \eta} = \frac{1}{Pe}\,\boldsymbol{\nabla}.[D(H)\boldsymbol{\nabla} H], \qquad \mathbf{x} \in \Omega(\eta), \tag{12}$$

$$-D(H)\,\frac{\partial H}{\partial n} = \overline{B}_{\text{gas}}(T(H) - \overline{T}_{\text{gas}} + Pe\,\overline{x}_{\mathbf{x}_P}(H - \overline{H}_{\text{spray}}), \quad \mathbf{x} \in \partial\Omega(\eta) : z > 0, \tag{13}$$

$$\frac{\partial H}{\partial r} = 0, \qquad r = 0, \tag{14}$$

$$D(H)\,\frac{\partial H}{\partial z} = \overline{B}_{\text{collector}}(T(H) - \overline{T}_{\text{collector}}), \qquad \mathbf{x} \in \partial\Omega(\eta) : z = 0, \tag{15}$$

$$H(\mathbf{x}, \eta_0) = H_0(\mathbf{x}), \qquad \mathbf{x} \in \Omega(\eta_0). \tag{16}$$

These equations are derived formally by a rescaling of the time with ϵ to give the slow-time variable η and by time-averaging the surface heat fluxes. The surface velocity $\overline{v}_{\mathbf{x}_P}$ is defined by

$$\overline{v}_{\mathbf{x}_P} = -\frac{\partial F_0}{\partial \eta}|\boldsymbol{\nabla} F_0|^{-1},$$

where $F_0(\mathbf{x}, \eta) \sim F(\mathbf{x}, \eta, t) + O(\epsilon)$ is an axisymmetric (slow-time) approximation to the solution of (10). Correspondingly, $\Omega(\eta)$ denotes the billet volume which is computed by following the evolution of $F_0(\mathbf{x}, \eta)$. An axisymmetric cylindrical coordinate system $\mathbf{x} = (r, z)$ is defined as in Figure 1, and it is assumed that the solution H to (12)–(16) is axisymmetric, *i.e.* $H(\mathbf{x}, \eta) = H(r, z, \eta)$. This clearly will only be justified if the boundary and initial conditions are also assumed axisymmetric.

2.3. Interpretation of the slow-time equations

Consideration of (12)–(16) could be motivated by simplicity, by the observation that billets are axisymmetric or by computational economy, (note that direct numerical solution of (1)–(4) and (10) would not be feasible). The more mathematical motivation and interpretation of (12)–(16) is that the slow-time heat-flow equations constitute the outer solution of an asymptotic

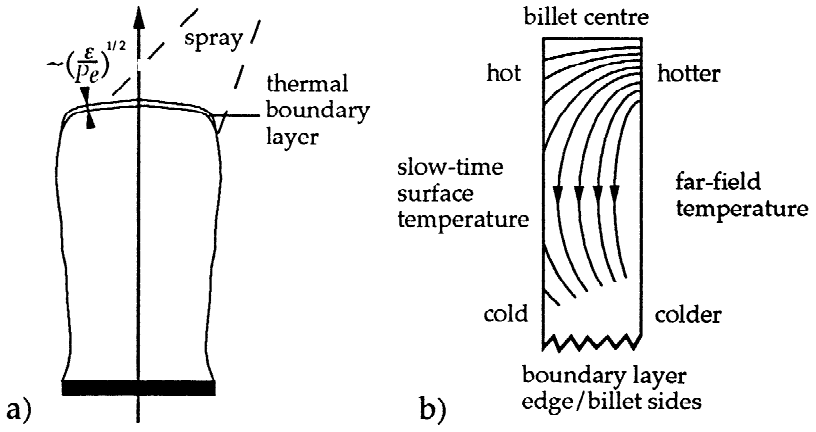

Figure 2. Schematic of the thermal boundary layer in a spray-formed billet; a) location, b) direction of heat flow in the matching layer.

approximation to H. This is hard to demonstrate rigorously, but may be justified heuristically as follows.

Unlike the time-averaged billet growth equations, the time-averaged heat-flow equations cannot provide a uniformly valid $O(\epsilon)$ approximation to the temperature field within the billet. In the first part of this paper, it was indicated [19] that the heat fluxes close underneath those parts of the billet surface upon which there is significant deposition are governed by a boundary-layer approximation. In this approximation, $O_S(1)$ transients in H can exist on the fast timescale t and will therefore destroy the uniformity of (12)–(16).

The thickness of this thermal boundary layer is $\sim (\epsilon/Pe)^{1/2}$. What is interesting is that this boundary layer is attached to the moving billet surface, (see Figure 2a), and exists effectively only because of relatively rapid surface growth on the fast timescale. For this reason, as well as the usual spatial limitations, there are temporal limitations to the validity of the boundary-layer approximation. These limitations arise since the boundary-layer approximation moves with the surface normal velocity and, after a sufficiently long time, $O(1)$ changes in the billet shape local to the boundary-layer coordinates will occur (even if the surface maintains a steady-state shape). For practical purposes, these limitations are irrelevant, since one does not wish to study boundary-layer heat flow over an extremely long time period. What the temporal limitations do suggest, however, is that the outer solution, to which the boundary-layer approximation should be matched, exists over both a longer timescale and a longer length-scale.

The "time-averaged" interpretation of the outer solution is further motivated by the findings, in [19], that the far-field enthalpy value in the boundary-layer approximation may be computed from time-averaging the surface heat fluxes and that departure of the boundary-layer transient from this far-field enthalpy value remains bounded.

Matching between the boundary-layer approximation and the slow-time solution to (12)–(16) is not considered, although the framework of a matched asymptotic approximation is believed to be the correct one within which to view (12)–(16). As intimated in Section 1, our reason for considering (12)–(16) is for practical application. The boundary-layer approximation in [19] and the slow-time equations (12)–(16) are valid over distinctly different timescales and length-scales, which are relevant to different thermo-physical processes within the billet. Matching would involve the use of an intermediate timescale and length-scale. Unless this

intermediate timescale and/or length-scale is relevant to a thermo-physical process within the billet, which is both of interest and cannot be adequately studied with either of the other two approximations, then there is no reason to undertake the matching process. A second objection to matching is that, although the spatial limits of the boundary-layer approximation are reasonably well defined in the direction normal to the surface, they are less well defined in the direction tangential to the surface.

A last, but essential, comment is that, if the end aim of the analysis is to be a uniformly valid asymptotic approximation to H, then matching is absolutely necessary. The surface enthalpy of the slow-time equations satisfies (13). The far-field enthalpy in the boundary-layer equations is found from the solution H of

$$0 = \overline{B}_{\text{gas}}(T(H) - \overline{T}_{\text{gas}}) + Pe\,\overline{v}_{\mathbf{X}_P}(H - \overline{H}_{\text{spray}}). \tag{17}$$

These two values are clearly different and matching is therefore necessary. The physical interpretation is that, on the fast timescale, the $O_S(1)$ enthalpy gradients deep within the billet are unable to affect heat flow close to the surface, where the short boundary-layer length-scale is relevant. At surface points where there is considerable deposition, (*e.g.* near the centre of the billet). the far-field boundary-layer enthalpy will be greater than the time-averaged surface enthalpy, (since (17) neglects conduction into the billet). At other surface points where there is much less deposition (*e.g.* approaching the sides of the billet), the far-field boundary-layer enthalpy will be smaller than the time-averaged surface enthalpy. Therefore, it is likely that significant heat flow will occur in the matching layer, (see Figure 2b). In the extreme case of zero deposition, (17) predicts that the far-field boundary-layer enthalpy is that which corresponds to the gas temperature, which is wrong. From this short discussion, it is apparent that both approximations, when used alone, must be used with appropriate caution.

3. Computational algorithm

To make progress in analysing (12)–(16), a computational solution is needed. Both (12) and the boundary conditions (13) and (15) are nonlinear. The problem is hard computationally, because the billet surface must be tracked as well as the solidus isotherm, *i.e.* this is a moving-boundary problem within a moving boundary. Billet shapes are not always simple, (*e.g.* exact cylinders), even when they are axisymmetric. Considerable effort is devoted towards controlling the shape of spray-formed billets, (see *e.g.* [25]), but significant variations from a constant radius and a steady billet crown shape may still occur during production. Therefore, although simpler model problems could be investigated, (*e.g.* linear heat conduction, $D =$ constant, and/or one-dimensional growth), these are of limited practical value. What is required here is a computational method which, (apart from the usual requirements of numerical stability), is robust enough to be able to cope with the real range of billet geometries.

With current computational capabilities, timing is not necessarily critical. However, for the purpose of undertaking parametric model studies one wants to wait only minutes, not hours. A reasonably fast numerical algorithm also opens up exciting new possibilities, such as coupling computations with a real-time (model-based) solidification-control algorithm. Lastly, it should be mentioned that excessive accuracy, in terms of a very high order of approximation and/or a very fine computational grid, will not be needed. Exceptionally high resolution would only be required if large temperature fluctuations are likely over very small length-scales in the slow-time problem (12)–(16). Due to the scaling used, all variables are expected to be $O(1)$ initially. Since $D(H) > 0$ is bounded, the problem remains parabolic (*i.e.* dissipative) and

because there are no internal heat sources, it is reasonable to suppose that the solutions remain (at least) as regular as the initial conditions. Large rapid transient thermal gradients will exist only in the boundary-layer model [19].

3.1. ALGORITHM DESCRIPTION

Motivated by the above discussion, the computation was carried out using a four-stage two-level, fully implicit finite-difference method. A fixed, uniformly regular grid, (spacing $\Delta r = \Delta z$), was used in both r- and z-directions. In the final stage of the algorithm, at each time step $\eta = \eta_n$, an iterative solution is found to the standard 6-point (two time level) fully implicit finite-difference approximation to (12). Stability and convergence of this method for a nonlinear parabolic equation such as (12), on an arbitrary smooth region, and with mixed boundary conditions, has been considered by Samarskii [26]. A generalisation to the case of an expanding domain has not been found in the literature. Due to the nonlinearity, there is a practical time step constraint of form $\Delta\eta \sim \frac{1}{2}\Delta z$, except in periods of rapid surface growth. Local truncation errors are $O(\Delta z) + O(\Delta\eta_n)$ near the billet surface and $O(\Delta z^2) + O(\Delta\eta_n)$ internally. This algorithm is described in considerable detail in chapter 7 of [20]; here only the significant points are mentioned. Issues relating to choice of this method are also discussed in [20].

Compared with an explicit method, where the time step restriction would be $\Delta\eta_n \sim \frac{1}{4}\Delta z^2$, the implicit algorithm requires approximately $(2 + k)$ times as many floating-point multiplications per meshpoint on each time step, where k is the number of iterations of the final stage of the algorithm. Supposing the model is integrated over the interval $\eta \in [0, \eta_{\text{end}}]$, the total CPU cost for the explicit method is $\propto \eta_{\text{end}}^2/\Delta z^4$ and that for the implicit algorithm is $\propto \eta_{\text{end}}^2/\Delta z^3$. For $\Delta z < 2/(2 + k)$ the implicit algorithm should be more efficient.

3.2. MODEL CLOSURE

Billet spray-forming is a longitudinal process, consisting of many complex interdependent sub-processes. To complete the model, at least for the purpose of computation, some of these sub-processes must also be modelled in order to give the parameters in the boundary conditions (13) and (15). For computing the billet-surface normal velocity, the model developed in [20, 21] was used. In [23], this model has been shown to reliably produce realistic results when simulating real billet growth. The other boundary-condition parameters are provided through the following sub-models.

3.2.1. *Treatment of the collector*

The collector typically consists of a cylindrical plate of material, which is securely fastened to the rotating hydraulic ram beneath it. The material is assumed to have constant density, specific heat capacity and thermal conductivity denoted by $\hat{\rho}_{\text{collector}}, \hat{c}_{\text{collector}}$ and $\hat{K}_{\text{collector}}$, respectively. The collector radius and thickness are denoted by $\hat{R}_{\text{collector}}$ and $\hat{Z}_{\text{collector}}$. It is assumed that the collector is initially at a uniform temperature, $\hat{T}^0_{\text{collector}}$.

The collector plate is thin and thermal contact between the base of the plate and the hydraulic ram is often poor (although it could be improved/controlled). Therefore, the sides and bottom of the collector are modelled as insulated. The collector will act as a heat sink for

the spray that is initially deposited and should then diminish in importance as the billet grows larger, and as it itself heats up.

Temperature profiles within the collector are computed using a completely standard 6-point explicit, centrally differenced finite-difference scheme, with a coarser spatial mesh than that which is used for the billet heat-flow computation. If necessary, time is advanced from η_n to η_{n+1} over a number of smaller substeps when computing the collector temperature, in order to preserve the stability of the explicit scheme. For computations carried out in this paper, it is assumed that the collector is made from an aluminium alloy with thermo-physical parameters $\hat{\rho}_{\text{collector}} = 2560\,\text{kg/m}^3$, $\hat{c}_{\text{collector}} = 1300\,\text{J/kg/C}$, $\hat{K}_{\text{collector}} = 180\,\text{W/m/C}$. An initial temperature $\hat{T}^0_{\text{collector}} = 25\,\text{C}$, and dimensions $\hat{R}_{\text{collector}} = .15\,\text{m}$ and $\hat{Z}_{\text{collector}} = 0.3\,\text{m}$ are also assumed. The thermal contact between the billet base and collector plate is assumed imperfect due to the rapid cooling and shrinkage of the first layers of spray depositing on the collector (this is easily verified by observation at the end of a process run); a value for $\hat{h}_{\text{collector}}$ in the range $1000 - 2000\,\text{W/m}^2/\text{C}$ is thought to be reasonable.[2]

3.2.2. $\overline{H}_{\text{spray}}$, $\overline{T}_{\text{gas}}$, *and* $\overline{B}_{\text{gas}}$

Derivation of fully accurate submodels to describe $\overline{H}_{\text{spray}}$, $\overline{T}_{\text{gas}}$, and $\overline{B}_{\text{gas}}$ is beyond the scope of this paper and there is also a lack of reliable measurements available. The assumption of constant $\overline{B}_{\text{gas}}$, $\overline{T}_{\text{gas}}$, and $\overline{H}_{\text{spray}}$ across the billet surface, which was made in [19] to study the boundary-layer approximation, cannot however be justifiably made when the entire billet is considered.

Most data is available concerning $\overline{H}_{\text{spray}}$. For given atomising gas pressures and metal mass-flow rates, the spray-fraction liquid, $f_{l,\text{spray}}$, is known to decrease with distance from the atomiser; (for measurements and computations see *e.g.* [4, 5, 6, 7, 9, 10, 11, 12, 13, 27, 28]). However, the exact spray-function liquid at a given distance from the atomiser nozzle will also depend on the local droplet size distribution and gas velocity, as well as on other process parameters, such as the melt superheat. More importantly, these results can also be alloy-dependent.

A very simplified model which roughly approximates the spray-fraction liquid variation with flight distance, as computed in [11] for representative process parameters and for a similar alloy composition to that considered here, is given by

$$f_{l,\text{spray}}(\hat{z}_d) = 1 - \hat{z}_d, \tag{18}$$

where $\hat{z}_d$ is the dimensional distance (in metres) from the atomiser nozzle. At typical flight distances, ($\hat{z}_d \approx 0{\cdot}5\,\text{m}$), the depositing spray is around 50% liquid and is cooling at approximately 1% liquid fraction per centimeter. This linear model is used to compute $\overline{H}_{\text{spray}}$ at the billet surface for all results presented.

Gas temperatures $\approx 100\,\text{C}$ are measured downstream from the billet, well after exiting the spray chamber. Within the spray-chamber temperatures will be significantly higher and in the absence of further data, a constant gas temperature

$$\hat{T}_{\text{gas}} = 200\,\text{C}, \tag{19}$$

close to the billet surface is assumed.

The heat-transfer coefficient $\hat{h}_{\text{gas}}$, is thought to decrease smoothly from a maximum value of approximately $1000\,\text{W/m}^2\text{C}$, directly under the spray on the billet crown, to a value in the

range $200 - 300\,\mathrm{W/m^2C}$ along the sides of the billet.[3] The transition from billet crown to billet sides typically occurs geometrically within a distance $\approx \hat{r}_s$ (denoting the radius of the metal spray) above the lower spray boundary, which is the line below which no spray lands, (see [20, 21]). The assumed variation in the gas heat-transfer coefficient is modelled very simply with a two parameter model. Heat-transfer coefficients $\hat{h}_{\mathrm{gas},1}$ and $\hat{h}_{\mathrm{gas},2}$ give the heat-transfer coefficients on the crown and sides of the billet, respectively. The transition between $\hat{h}_{\mathrm{gas},1}$ and $\hat{h}_{\mathrm{gas},2}$ is assumed to occur only within a distance $\hat{r}_s$ above the lower spray boundary. The variation is modelled as being proportional to the decay in the time-averaged spray mass-flux distribution, from its value a height $\hat{r}_s$ above the lower spray boundary, to zero at the lower spray boundary.

3.2.3. *Aluminium alloys*

A variety of aluminium alloys are used to manufacture spray-formed billets. The purpose of this paper is, however, not to explore intra-alloy variations. Therefore, the same aluminium alloy will be used as has been used in the first part of this paper [19]. To aid the reader, the thermophysical data for this alloy are reproduced in Table I at the end of the paper. The nonlinear functions $T(H)$ and $D(H)$ are shown in Figure 2 of [19].

3.2.4. *Dimensionless model parameters*

For a typical $\hat{R} = 150\,\mathrm{mm}$ radius billet and the aluminium alloy of Table I, the following dimensionless model parameters are considered realistic and are used for all following computations (unless otherwise stated).

$$\begin{aligned} \overline{T}_{\mathrm{gas}} &= -3{\cdot}755, & \overline{B}_{\mathrm{gas},1} &= 0{\cdot}8, & \overline{B}_{\mathrm{gas},2} &= 0{\cdot}25, \\ r_{\mathrm{collector}} &= 1{\cdot}0, & z_{\mathrm{collector}} &= 0{\cdot}2, & \overline{T}^{0}_{\mathrm{collector}} &= -5{\cdot}67, \\ \overline{B}_{\mathrm{collector}} &= 1{\cdot}6, & Pe &= 1{\cdot}8. \end{aligned}$$

The spray cone radius $r_s = 0{\cdot}5$ and the spray oscillates between angles $[a_1, a_2] = [28{\cdot}5^\circ, 41{\cdot}5^\circ]$ according the scanner angle function shown in Figure 2 of reference [23].

3.2.5. *Initial conditions*

Setting of initial conditions at $\eta_0 = 0$, when there is no spray-formed deposit, is obviously problematic, but also is necessary for computation to proceed. Within the computational algorithm, in order that a discretised form of (13) may be satisfied on the billet top surface, it is necessary to prescribe initial values on at least two gridlines internal to the billet. Therefore, initial conditions for the numerical solution are set by assuming an initially uniform deposit of thickness $2\Delta z$ and radius r_c on top of the collector plate. The collector plate initial vertical displacement below the atomiser is increased by a distance $2\Delta x$, so as to leave the billet-growth computation completely unaffected. Prescription of initial conditions in this way clearly introduces an initial error of $O(\Delta z)$ into the solution.

The initial vertical enthalpy gradient through the initial deposit is assumed to be linear, a discretised form of (13) is satisfied at the top surface and it is assumed that the mean enthalpy of the initial layer $\overline{H}_i$ is given by the heat fluxes through the top surface and to the collector, *i.e.*

$$0 = \overline{B}_{\mathrm{collector}}[T(\overline{H}_i) - \overline{T}_{\mathrm{collector}}] + \overline{B}_{\mathrm{gas}}[T(\overline{H}_i) - \overline{T}_{\mathrm{gas}}] + Pe\,\overline{v}[\overline{H}_i - \overline{H}_{\mathrm{spray}}]. \tag{20}$$

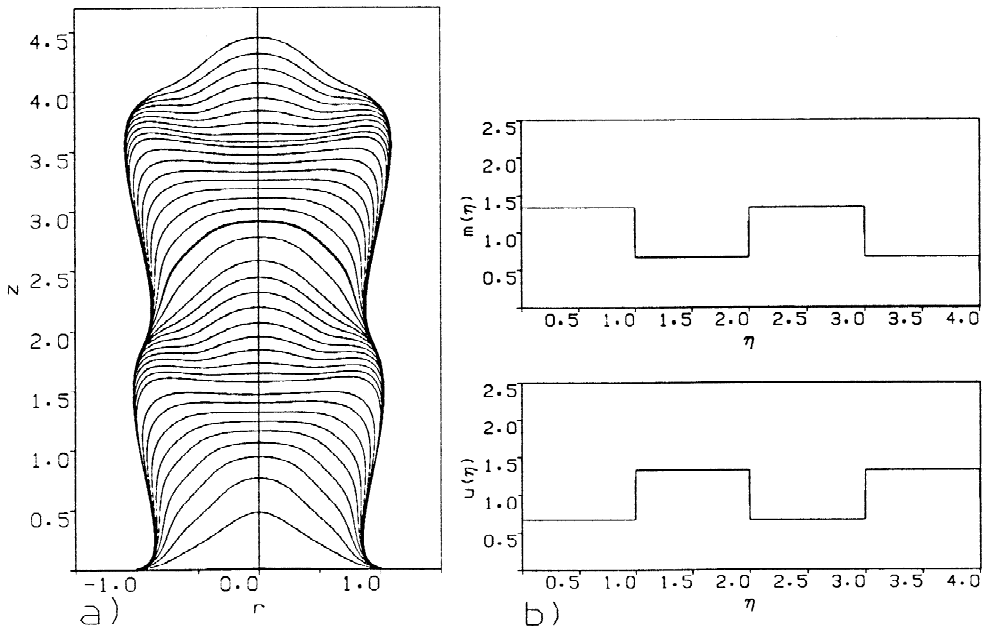

Figure 3. Test billet computation, isotherms plotted at: a) $\eta = 0{\cdot}5$, b) $\eta = 0{\cdot}2$, c) $\eta = 1{\cdot}5$, d) $\eta = 2{\cdot}0$, e) $\eta = 2{\cdot}5$, f) $\eta = 3{\cdot}0$, g) $\eta = 3{\cdot}5$, h) $\eta = 4{\cdot}0$.

3.3. TEST PROBLEM

In order to examine the performance of the algorithm, a challenging test problem is considered. During a production run, shape control is affected by variation of the metal mass flow rate through the atomiser $\dot{m}(\eta)$, and the withdrawal speed of the collector vertically downwards, $u(\eta)$. A properly robust algorithm must be able to cope with the following.

1. Sharp and significant changes in both $\dot{m}(\eta)$ and $u(\eta)$ during the process run.
2. Wide spatio-temporal variations in surface velocity, ($\Longrightarrow$ heat inflow).
3. Significant spatio-temporal variations in the other boundary conditions.
4. Billet growth at a range of different angles to the computational gridlines.
5. Challenging billet geometries.

For these reasons, the heat flow has been computed within the billet shown in Figure 3a. The different surfaces in Figure 3a show the surface of the (axisymmetric) billet plotted at time intervals $\Delta\eta = 0{\cdot}1$, throughout a process run of total length $\eta_{\text{end}} = 4$. The step changes in $\dot{m}(\eta)$ and $u(\eta)$ which have produced this strange billet are shown in Figure 3b.

A billet shape such as that in Figure 3a would require much wasteful machining to achieve a cylindrical shape suitable for extrusion and would almost certainly be rejected by a production quality control following micro-structural analysis. A model capable of computing the isotherms within such a billet, during formation, is thus of great value in providing insight into the real causes of production failure.

To compute the heat flow, a mesh spacing $\Delta r = \Delta z = 1/70$ has been used.[4] Figure 4 shows the isotherms within cross-sections of the axisymmetric billet, computed with the algorithm described. Figures 4a–h show the isotherms at intervals $\Delta\eta = 5$ throughout the modelled run. The solidus isotherm is marked with a fine dashed line and temperatures above

the solidus temperature are marked with a solid line at intervals corresponding to a 1% change in the alloy liquid fraction. Below the solidus temperature, isotherms are marked with a coarse dashed line at temperature intervals which are equivalent to 20% of the freezing range of the alloy, (the freezing range $\Delta\hat{T} = \hat{T}_l - \hat{T}_s = 91{\cdot}8$ C in this case). The same graphical notation is used throughout the paper.

Significant temperature transients can be observed in Figure 4. Throughout the process run the billet varies between being nearly fully solid, (Figures 4c, d, g and h), and containing significant volumes of semi-solid alloy (Figures 4a, b, e and f). In the semi-solid regions, the field equation (12) is extremely nonlinear. The isotherms in Figure 4 are smooth throughout the run, even close to the billet surface, thus demonstrating the capabilities of the algorithm in using a fixed, square mesh to cope with a boundary that is both curved and moving. It is clear that the nonlinearity causes no difficulties for the algorithm.

4. Numerical results

The aim of this section is to use the computational algorithm of Section 3 to investigate some practically relevant process situations.

4.1. START-UP STRATEGIES

When well controlled, for the major part of a production run, variations in the billet radius are minimal and the billet crown maintains a reasonably steady shape, when viewed in a frame of reference fixed relative to the atomiser height. This mode of production is highly desirable, (see *e.g.* discussions in [20, 21, 22, 25]). However, at the start of the production run, there is nearly always a period of significant unsteady transient growth. Billet growth in the initial phase of production runs has been considered in [23], where a number of different generic start-up strategies for controlling the initial growth period were examined. In [23], only billet growth was considered. Here, three representative strategies are reconsidered from the point of view of how the thermal behaviour of the initial deposit is affected by the different surface movements.

For a typical 0·15 m radius production billet and for Peclet numbers *Pe* in the range 1·4 – 1·8, the mean billet withdrawal speed $\hat{U}_0$ will be in the approximate range 0·5 – 0·65 mm/s and the slow timescale is about 230–300 s long. The start-up phase of the run is therefore assumed to be approximately equal to the time period $\eta \in [0, 1]$, (*i.e.* the first 4 – 5 minutes of a normal production run).

4.1.1. *Delayed billet withdrawal*

Here the collector height is kept stationary for a given initial delay interval, while the plant operator observes the development of a suitable crown profile on a video monitor. Typically, the centre of the billet grows upwards first into a "hat" shape and then, when the billet radius is observed to "fill out" a bit more, the operator commences billet/collector withdrawal. Here the mass flow rate is assumed constant, $\dot{m}(\eta) = 1$, and the withdrawal velocity $u(\eta)$ is given by

$$u(\eta) = \begin{cases} 0, & 0 \leq \eta \leq 1, \\ 1, & 1 < \eta. \end{cases} \tag{21}$$

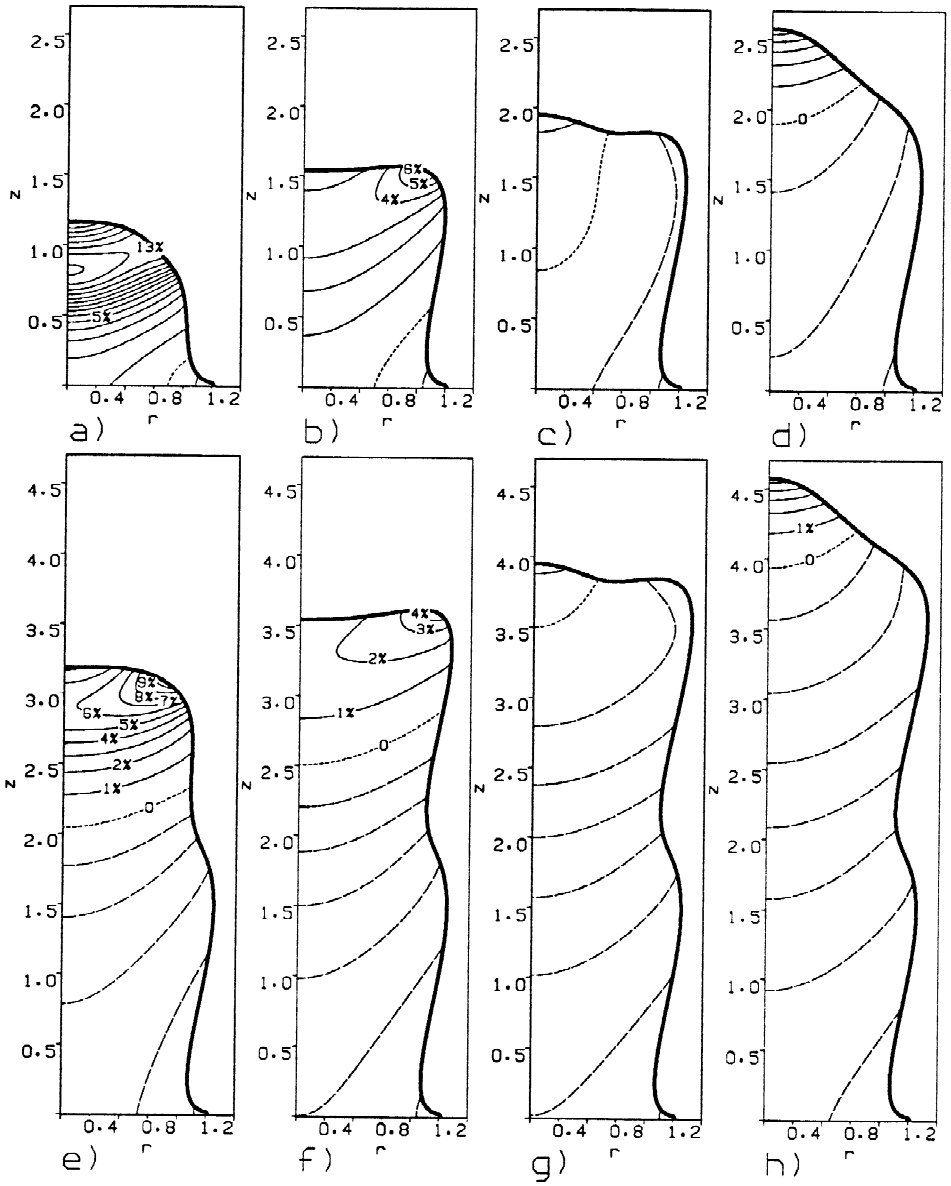

Figure 4. Delayed billet withdrawal: a) $\eta = 0{\cdot}1$, b) $\eta = 0{\cdot}2$, c) $\eta = 0{\cdot}4$, d) $\eta = 0{\cdot}6$, e) $\eta = 0{\cdot}8$.

The collector is initially positioned a height $z_n = 3$ below the atomiser nozzle. These conditions are exactly as for the billet growth modelled in reference [23].

Results are shown in Figure 5 for times $\eta = 0{\cdot}1, 0{\cdot}2, 0{\cdot}4, 0{\cdot}6, 0{\cdot}8$ It can be seen that the billet surface grows initially very rapidly in the centre, until about $\eta = 0{\cdot}4$ (compare Figures 5a and b with Figure 5c). This is followed by a period of slower growth of the billet centre, as the billet edge grows up into the spray. The initial growth surge results in fraction liquids of over 20% near the billet centre, whereas the very outside of the billet (where little spray is deposited) is chilled rapidly and effectively by the collector. In these first stages of growth, thermal gradients tangential to the surface, between the centre and edge of the billet, are $\approx$ 1300 C/m.

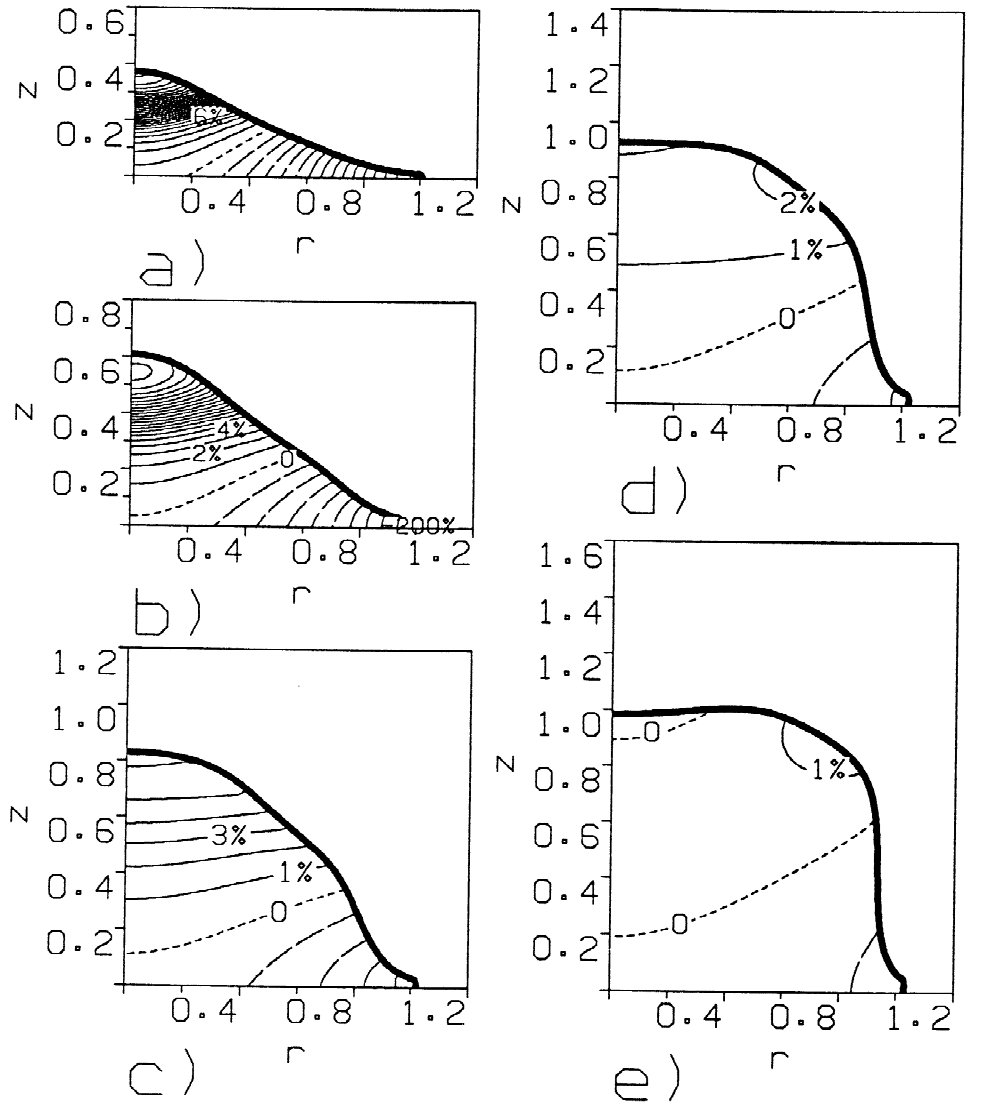

Figure 5. Delayed billet withdrawal: a) $\eta = 0{\cdot}1$, b) $\eta = 0{\cdot}2$, c) $\eta = 0{\cdot}4$, d) $\eta = 0{\cdot}6$, e) $\eta = 0{\cdot}8$.

A number of things should be said about these results. Firstly, they are believed to be quite realistic. When initial billet growth is rapid and results in a significant "hat-shaped" deposit, (as in Figures 5a and b), the billet centre is observed to glow brightly on the video monitor and pyrometer readings can also register the higher surface temperatures. Maintenance of such a large pool of semi-solid alloy over significant time periods will allow macro-segregation to occur. This is, however, probably irrelevant here, since the large thermal gradients are likely to lead to shrinkage defects which will make the billet unsaleable. Usually, due to the incremental nature of spray-formation, shrinkage defects are minimal, seriously affecting only the first few centimeters of the billet next to the collector. However, on occasion, "hot tears" are found in the base of the billet. These are large tears in the billet, often with a circumferential aspect. It is postulated that the likely cause of these defects is the development of thermal stresses, due to significant non-uniform thermal gradients, as shown in Figure 5. A final point of interest is

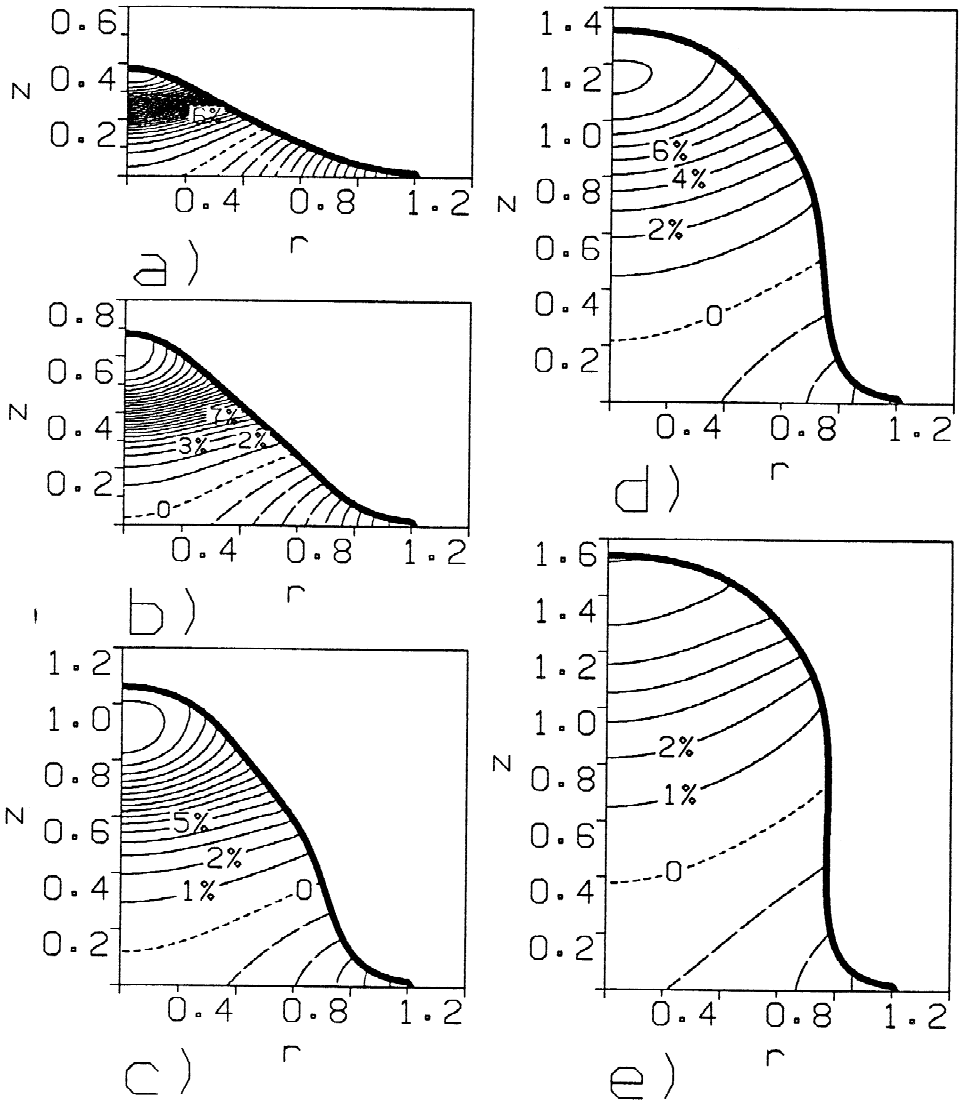

Figure 6. Immediate billet withdrawal: a) $\eta = 0{\cdot}1$, b) $\eta = 0{\cdot}2$, c) $\eta = 0{\cdot}4$, d) $\eta = 0{\cdot}6$, e) $\eta = 0{\cdot}8$.

that the thermal gradients are not monotone within the billet, (see the looped isotherm near the tip of the billet in Figures 5b and 5c, and note in Figure 5c that the isotherm near the billet tip is a 5% liquid-fraction isotherm; the maximum temperature is within the billet). This indicates the possibility of solute-trapping on a macroscopic scale.

4.1.2. *Immediate billet withdrawal*

Rapid vertical growth of the billet centre might intuitively be thought to result from delaying the withdrawal of the billet, *i.e.* moving the billet in the direction opposite to the surface growth should reduce the surface growth. This intuition is, however, completely wrong.

With the same parameters as above, slow-time heat flow has been again computed for the initial phase of billet growth, but now with constant withdrawal velocity, $u(\eta) = 1$. The results are shown in Figure 6, which can be compared directly with Figure 5. It is seen that

for $\eta \in [0, 0.2]$ billet growth and solidification is very similar to that in Figure 5, with large thermal gradients developing and significant liquid fractions persisting near the billet centre. The reason for this counter-intuitive result is that the effect of withdrawing the billet earlier is to maintain the billet top surface at a position, relative to the atomiser height, where the density of the spray mass flux is greater. Therefore, the vertical growth of the billet centre is actually faster here than in Section 4.1.1. Further away from the billet axis of rotation, the withdrawal motion does remove the billet from the region where the spray mass-flux density is large and surface growth is consequently retarded. At the later stages of this initial period, the immediately withdrawn billet is rather tall and thin, whereas the delayed billet is shorter, but does fill out to a radius $r_b \approx 1$. Note that the same mass has been deposited in both cases.

In the final stages of the start-up phase, the vertical growth of the centre is reduced, but is still sustained relative to the edges of the billet. Consequently, the high-fraction liquid in the billet is sustained longer than in the delayed-withdrawal billet. Again non-monotone thermal gradients are found in the billet, (Figures 6c and d). As in Section 4.1.1, these are caused by an initial acceleration of the billet centre, followed by a deceleration as the spray density reduces.

4.1.3. *Optimal collector positioning*

Without even considering heat flow, the billets resulting from the start-up strategies in Sections 4.1.1 and 4.1.2 are not acceptable from the point of view of the amount of billet which must be machined, in order to produce a perfect cylinder for post-processing. The start-up strategy proposed in [23] for controlling the initial phase was to optimally position the collector and withdraw the billet immediately. Optimal positioning, from a dynamic point of view, is achieved when $z_n \approx 2\frac{1}{3}$.

Computations for this case are shown in Figure 7. The remaining parameters are exactly as in Section 4.1.2. This start-up strategy is found to produce much more uniform heat fluxes within the billet than in Figures 5 and 6. To begin with, the spray is effectively chilled by the collector, even at the centre. In contrast to the other start-up strategies, the billet crown shape changes only slowly and reasonably uniformly across the billet radius. Centre-to-edge thermal gradients peak here at $\approx$ 600 C/m, (*i.e.* about half as large as in Sections 4.1.1 and 4.1.2). The thermal gradients also remain monotone. Peak fraction liquids of little over 2% are found in the latter stages of the start-up phase (see Figure 7e).

It is noted here that the higher initial positioning of the collector means that the spray arriving at the billet surface is actually considerably hotter than in Sections 4.1.1 and 4.1.2, (*i.e.* containing about 10% more fraction liquid). In spite of this, the billet is much colder. This demonstrates clearly that it is the billet growth which controls the heat fluxes in Sections 4.1.1 and 4.1.2.

4.2. STEADY-STATE HEAT FLOW

The dynamics of billet growth on the slow timescale are well understood: *i.e.* mathematically [20, 21], computationally [22, 23], and from the shape-control point of view [25]. The dominating feature of billet-growth dynamics is the existence of a stable steady-state shape, which the top part of the billet grows towards. The dominant effect of billet growth in determining the thermal behaviour, shown clearly by the results in Section 4.1, leads one to question whether

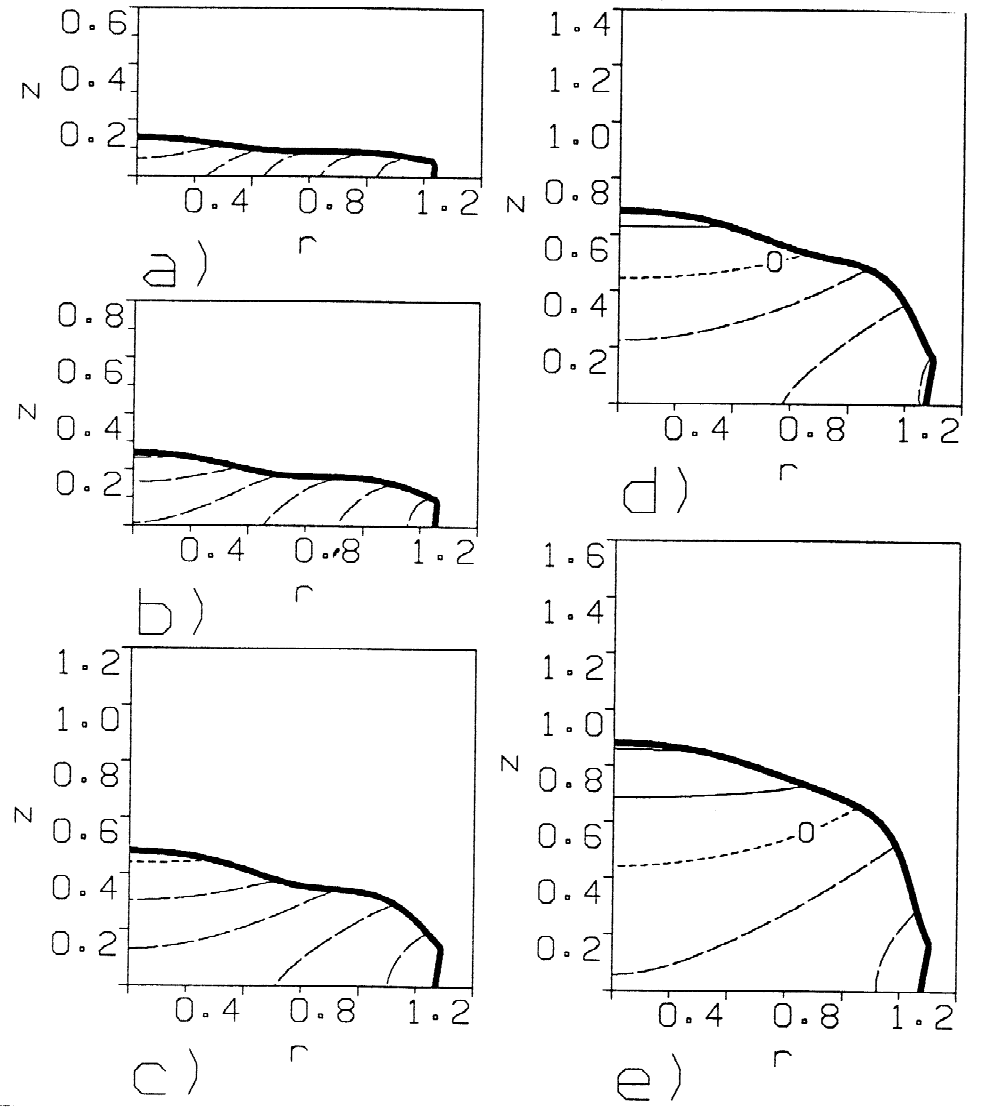

Figure 7. Initial collector position: $z_n = 2\frac{1}{3}$: a) $\eta = 0{\cdot}1$, b) $\eta = 0{\cdot}2$, c) $\eta = 0{\cdot}4$, d) $\eta = 0{\cdot}6$, e) $\eta = 0{\cdot}8$.

the thermal behaviour within the billet becomes steady in some sense when the geometric behaviour of the billet also becomes steady.

To investigate this, the computations in Section 4.1 have been continued for $\eta \in [0, 3]$ and are shown in Figures 8, 9 and 10, corresponding to Sections 4.1.1, 4.1.2 and 4.1.3, respectively. Note that for $\eta \geq 1, \dot{m}(\eta) = 1$ and $u(\eta) = 1$ in all three computations. The thermal and geometric conditions at $\eta = 1$ are quite different in each computation, as seen in Figures 8a, 9a and 10a. However, by time $\eta = 3$, the crown of the billet has grown to a similar shape in each computation (see Figures 8c, 9c and 10c). Additionally, it can be seen that the isotherms in the very top of the billet crown become progressively more similar. The heat flow in the lower part of the billets, however, remains quite different, (as does the geometry). A continuation of the computations still further shows that the enthalpy field in the billet crown converges to an enthalpy field which appears to remain steady, within a spatial coordinate

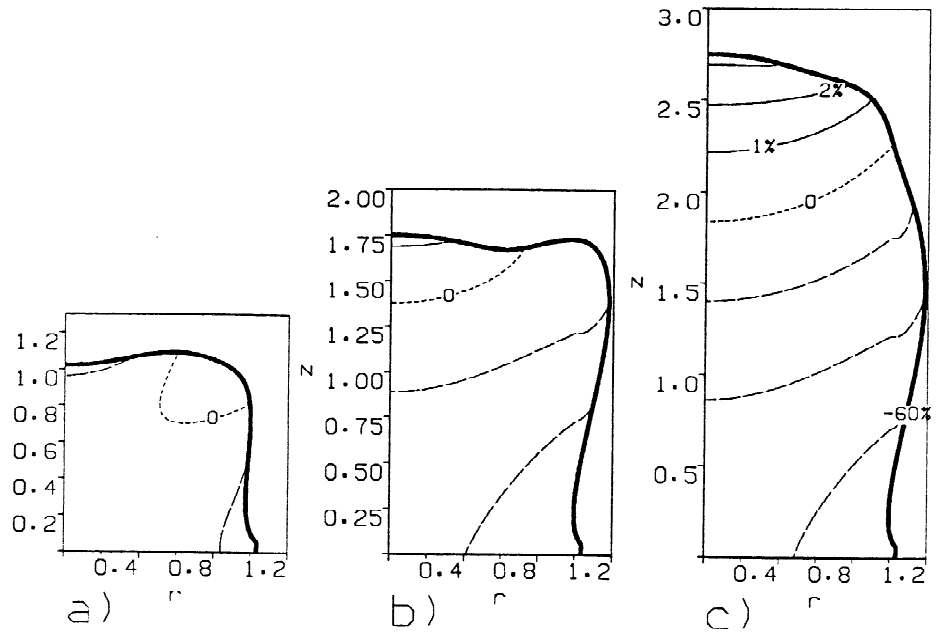

Figure 8. Delayed billet withdrawal: a) $\eta = 1{\cdot}0$, b) $\eta = 2{\cdot}0$, c) $\eta = 3{\cdot}0$.

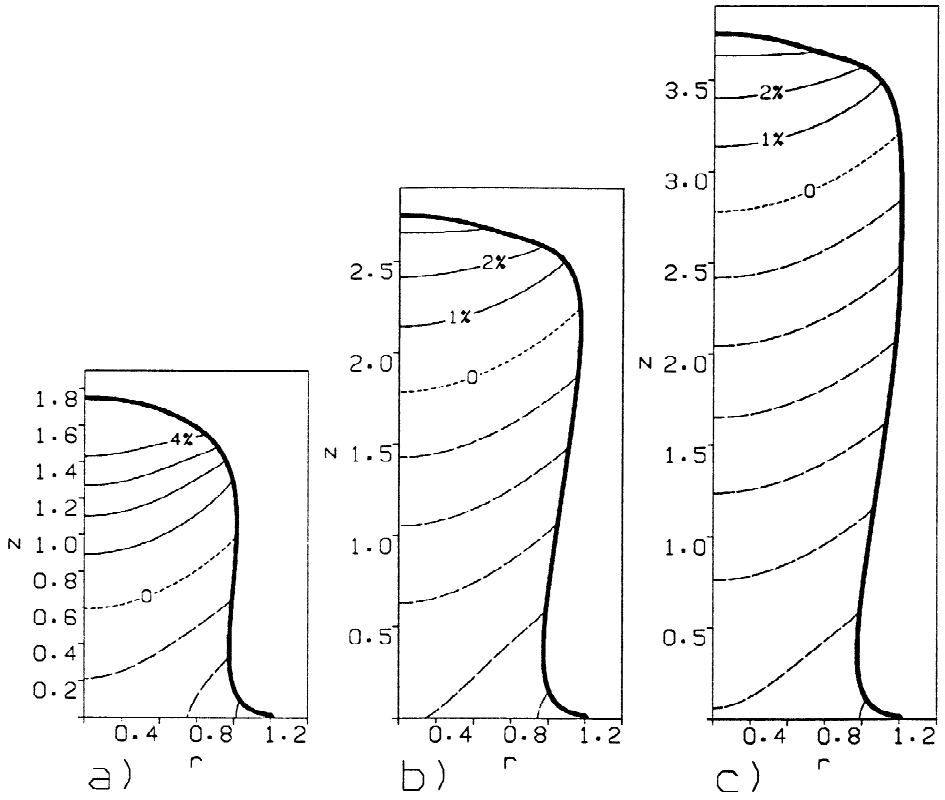

Figure 9. Immediate billet withdrawal: a) $\eta = 1{\cdot}0$, b) $\eta = 2{\cdot}0$, c) $\eta = 3{\cdot}0$.

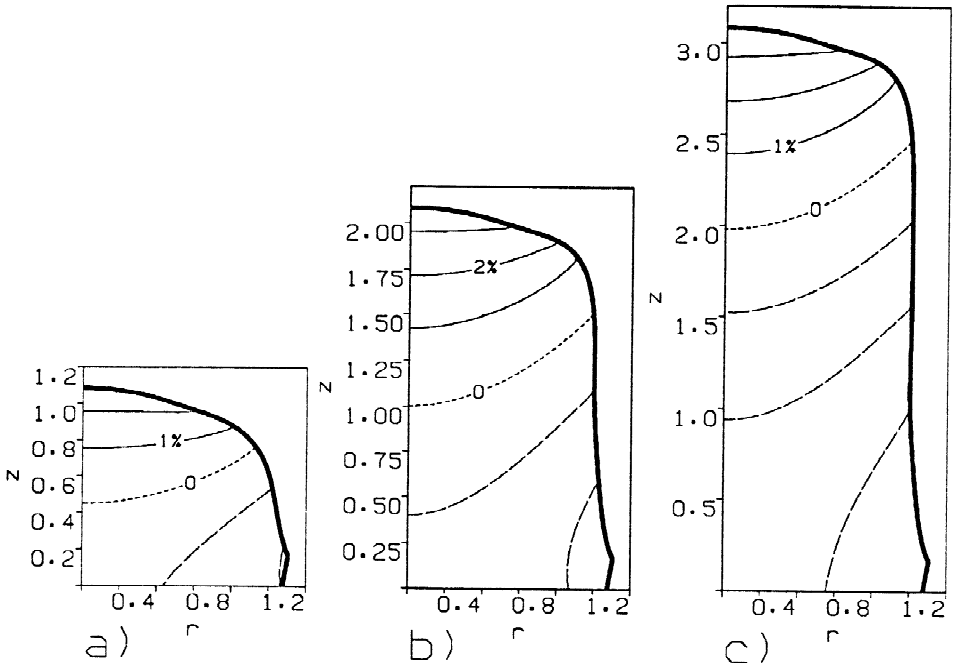

Figure 10. Initial collector position, $z_n = 2\frac{1}{3}$: a) $\eta = 1{\cdot}0$, b) $\eta = 2{\cdot}0$, c) $\eta = 3{\cdot}0$.

system which is fixed relative to the atomiser height. Only the computations for the optimally positioned collector are shown (see Figure 11).

The importance of steady-state heat flow in the billet crown is as follows. Suppose two horizontal slices are taken through the billet, at fixed heights z_a and z_b above the collector plate. The alloy which is at the same radial distance r in each of the two slices will experience the same thermal history, apart from a time delay, and can therefore be expected to have similar microstructural properties, (*i.e.* steady-state heat flow implies microstructural homogeneity in the z-direction for the end product). The same will not be true in the radial direction, since there is always a radial enthalpy gradient. However, the thermal histories at different radial positions within the same horizontal slice will also be quite similar, (*e.g.* rates of cooling).

Existence of steady-state enthalpy fields is not hard to understand heuristically. Moving to a coordinate system which is fixed at a set vertical distance below the atomiser height, Equation (12) becomes

$$\frac{\partial H}{\partial \eta} = u(\eta)\,\frac{\partial H}{\partial z_1} + \frac{1}{Pe}\,\boldsymbol{\nabla}.[D(H)\boldsymbol{\nabla}H], \quad \mathbf{x}_1 \in \Omega_1(\eta), \tag{22}$$

where $\Omega_1(\eta)$ denotes the domain of the billet in this "billet-crown" coordinate system, denoted by $\mathbf{x}_1$. As the geometry becomes steady, $\Omega_1(\eta)$ becomes a constant shaped domain, at least above say $z_1 = z^*$. The boundary conditions (13) and (14) remain unchanged by the transformation. The surface heat fluxes in (13) depend primarily on position of the surface relative to the atomiser, and can be expected to become steady with $\Omega_1(\eta)$. Therefore, it is only the heat flux across $z_1 = z^*$ which is important. If this heat flux becomes steady then, due to the dissipative nature of (22), one expects that the solution of (22) will converge to a steady state.

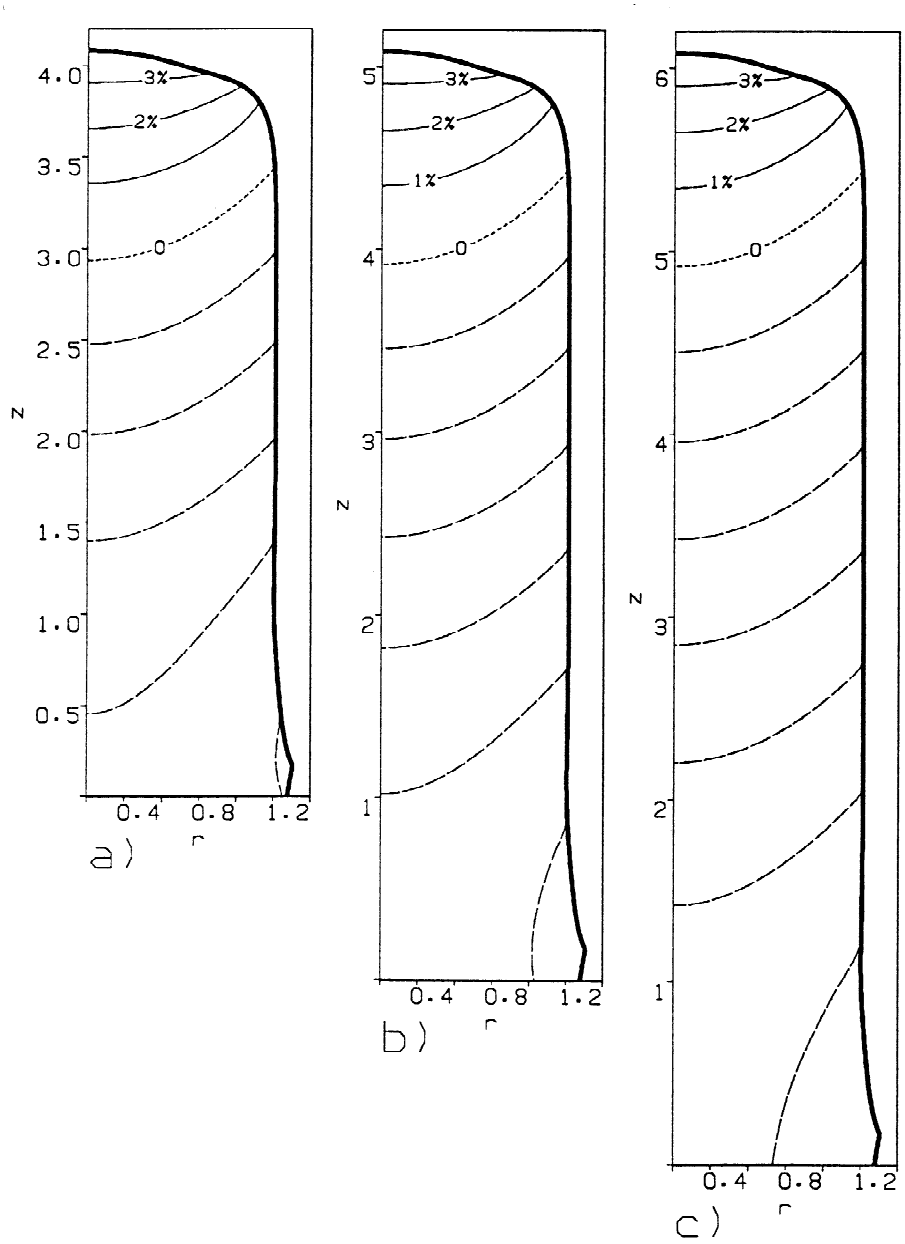

Figure 11. Steady-state heat flow in the billet crown: a) $\eta = 4{\cdot}0$, b) $\eta = 5{\cdot}0$, c) $\eta = 6{\cdot}0$.

Note that if the geometry below $z_1 = z^*$ is different between two billets, (*e.g.* due to different initial growth or to the use of collectors of different sizes, then the ratio of billet surface area to billet volume in the lower parts will be different and one would expect a different heat flux at $z_1 = z^*$. In fact, the existence of the collector as an initial geometry probably means that the heat flux at $z_1 = z^*$ never becomes properly steady, except in the limit of an infinitely long billet. From a practical point of view, the effect of the collector diminishes quite rapidly at the billet grows and the enthalpy field may as well be considered to approach a steady state.

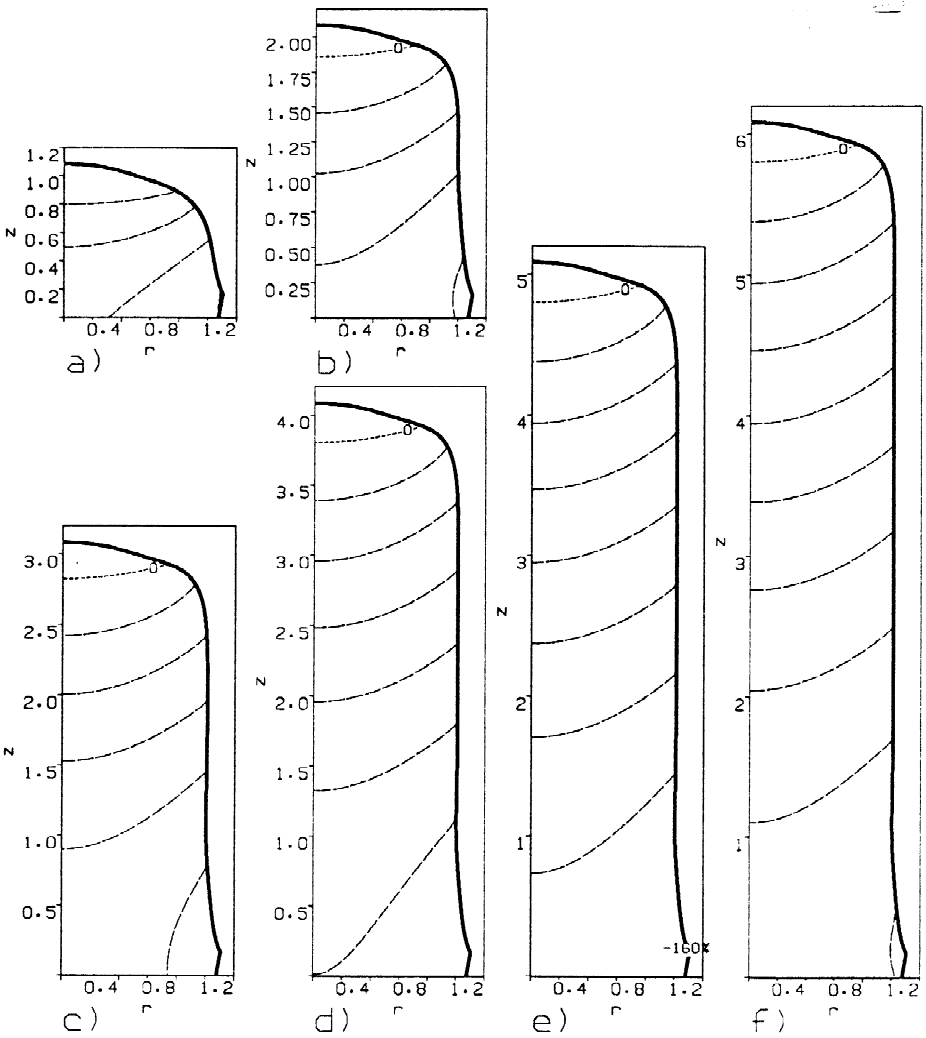

Figure 12. Steady-state heat flow. $Pe = 1{\cdot}4$: a) $\eta = 1{\cdot}0$, b) $\eta = 2{\cdot}0$, c) $\eta = 3{\cdot}0$, d) $\eta = 4{\cdot}0$, e) $\eta = 5{\cdot}0$, f) $\eta = 6{\cdot}0$.

4.3. CHANGING *Pe*

For the alloy considered here, the Peclet number during plant operation is usually in the range $Pe = 1{\cdot}4 - 1{\cdot}8$, (see [19], Figure 3). The Peclet number can be thought of intuitively as the ratio of timescales for conduction and for billet growth. From this perspective, decreasing *Pe* might be thought of in terms of allowing more time for the billet to solidify. Consequently, one expects that billets produced at lower values of *Pe* will be colder. This is indeed found to be the case.

Figure 12 shows the heat flow inside a billet produced for $Pe = 1{\cdot}4$. The initial conditions and subsequent growth are exactly as for the optimally positioned billet in Figures 7, 10 and 11. The computed results show again that the heat flow in the billet crown converges to a (pseudo) steady state quite rapidly, but the computed temperatures within the billet are colder throughout, than for the $Pe = 1{\cdot}8$ computation.

This is easily explained in terms of the transformed equation (22). A decrease in *Pe* is seen to lower the heat inflow into the billet, through the boundary condition (13), whilst increasing the effectiveness of conduction relative to convection in (22). Since the geometry is unchanged with *Pe* one is effectively just determining the heat fluxes at the lower boundary $z_1 = z^*$ of the steady-state crown domain. To appreciate this, note that, outside of the spray, the boundary conditions (13)–(15) will be unaffected by a change in *Pe*. Consequently, the surface heat fluxes in the lower part of the billet, both out through the surface and into the collector, should be unaffected by a change in *Pe*. Consequently, the surface heat fluxes in the lower part of the billet, both out through the surface and into the collector, should be unaffected by a change in *Pe*. Therefore, it is expected that the heat flux out of the steady billet crown and into the stem of the billet should also be relatively unaffected by a change in *Pe*. This intuition is confirmed by the very similar thermal gradients observed down the length of the billets in both Figures 11a–c and Figures 12d–f.

4.4. Steady shape and unsteady heat flow

Although geometric stability is often achieved in controlled production runs, this does not necessarily imply that $\dot{m}(\eta)$ and $u(\eta)$ are well controlled. In fact, considerable variations in both $\dot{m}(\eta)$ and $u(\eta)$ do occur in real production runs (see various examples in [25]). The problems in maintaining a steady $\dot{m}(\eta)$ and $u(\eta)$ usually stem from control of $\dot{m}(\eta)$, which is difficult for a number of technical reasons. The variations in $u(\eta)$ then follow from an attempt to keep the ratio $u(\eta)/\dot{m}(\eta)$ approximately constant (see [20, 21, 23, 25]). As a simulated example of this type of process condition, an in-phase $\pm$25% step variation in $\dot{m}(\eta)$ and $u(\eta)$ are a real process feature and this level of variation is quite realistic. Since the variation is in-phase, the ratio $u(\eta)/\dot{m}(\eta) = 1$ throughout the simulated process run. This implies that the billet crown geometry should remain steady, relative to billet-crown coordinates $\mathbf{x}_1$.

The computed billet cross-sectional isotherms are shown in Figures 13a–h and the functions $\dot{m}(\eta)$ and $u(\eta)$ are shown in Figure 13i. The billet crown does indeed maintain the same steady-state shape as previously. Note also that, due to the way in which the functions $\dot{m}(\eta)$ and $u(\eta)$ have been chosen, at the times $\eta = 1, 2, 3, 4$, the billet surface is in exactly the same position as it is at these same times in the earlier computations of Sections 4.2 and 4.3, (*i.e.* the same amount of mass has been deposited). Since the surface position relative to the atomiser is also maintained, the total heat inflow from the spray at these times is also identical with the earlier computations. Therefore, the effects seen in Figures 13a–h are only the result of the variation in $\dot{m}(\eta)$ and $u(\eta)$.

In Figures 13a–h one can observe a considerable thermal variation between periods in which the billet is hot or cold. Steady geometric behaviour does not imply steady thermal behaviour.

The physical explanation for the large changes in alloy liquid fraction, (*e.g.* see Figure 13e and Figure 13f) is as follows. Firstly, note that the geometry remains steady in a frame of reference which is fixed to the atomiser height. During time periods when $u(\eta)$ and $\dot{m}(\eta)$ are high (see Figure 13i), the billet is being withdrawn away from the atomiser relatively fast, more mass flows through the atomiser and deposits on the billet surface. Since the submodels which describe gas cooling effects are unaffected, the net effect is the deposition of more hot spray on the billet surface than during time periods when $u(\eta)$ and $\dot{m}(\eta)$ are low, (*i.e.* the billet heats up). Although, over the total length of the modelled run, the total heat inflow from the spray is identical with that in the earlier steady-state computations, there is a significant

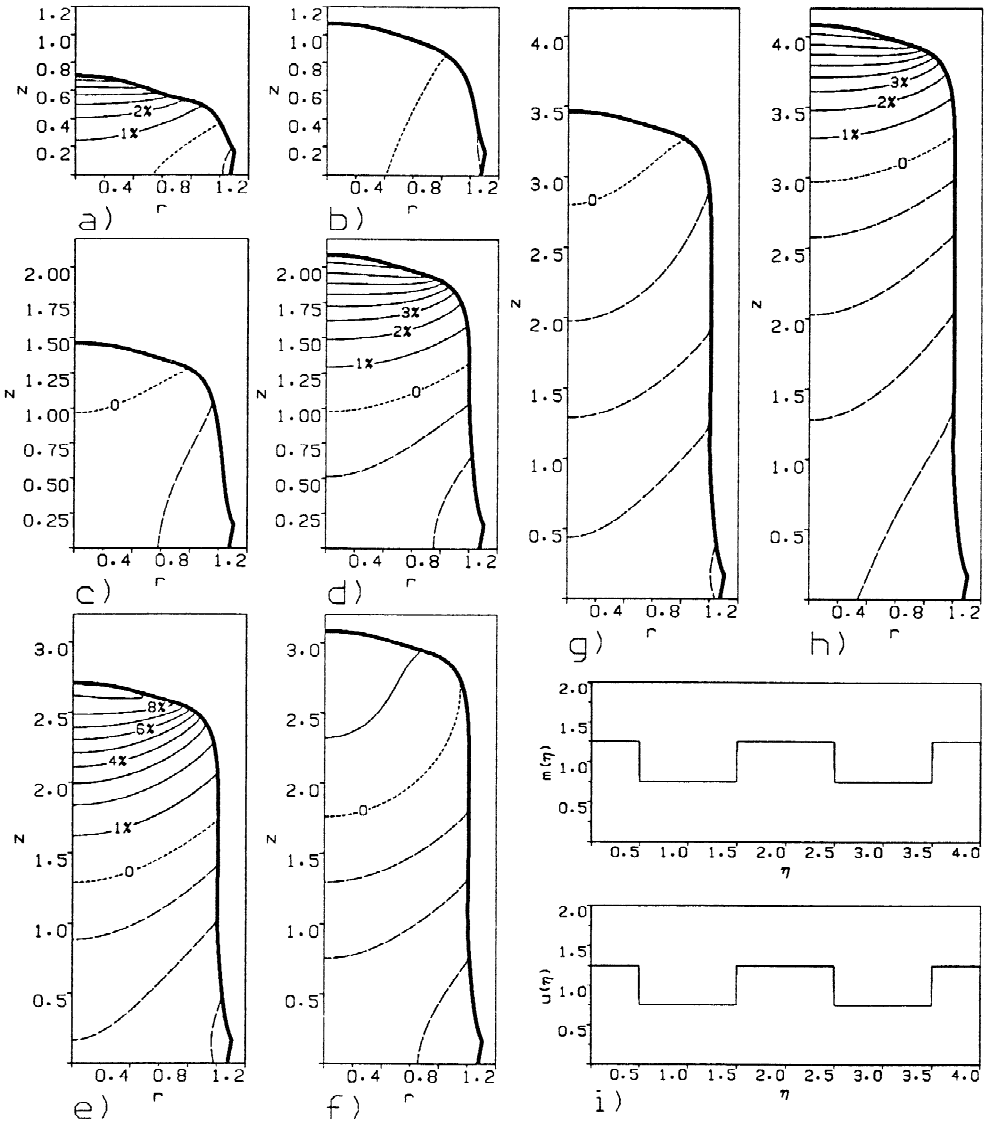

Figure 13. Steady crown geometry, unsteady heat flow, $Pe = 1{\cdot}8$: a) $\eta = 0{\cdot}5$, b) $\eta = 1{\cdot}0$, c) $\eta = 1{\cdot}5$, d) $\eta = 2{\cdot}0$, e) $\eta = 2{\cdot}5$, f) $\eta = 3{\cdot}0$, g) $\eta = 3{\cdot}5$, h) $\eta = 4{\cdot}0$, i) $\dot{m}(\eta)$ and $u(\eta)$.

temporal variation in exactly when the spray is deposited. As in Section 4.1, billet growth rates have a critical effect on billet temperature.

After the start-up phase of the computation, thermal transients are confined mostly to the billet-crown region. One interpretation of this variation is that the heat flow in the billet crown converges relatively quickly to a new thermal (pseudo) steady state, following step changes in $\dot{m}(\eta)$ and $u(\eta)$. If the heat fluxes further down the stem of the billet remain largely unaffected by the step change, (as seems reasonable), then the (pseudo) steady problem in the billet crown is defined by

$$0 = u(\eta)\,\frac{\partial H}{\partial z_1} + \frac{1}{Pe}\,\boldsymbol{\nabla}.[D(H)\boldsymbol{\nabla}H], \quad \mathbf{x}_1 \in \Omega_1, \tag{23}$$

and the boundary condition (13) can be written as

$$-D(H)\,\frac{\partial H}{\partial n} = \overline{B}_{\text{gas}}(T(H) - \overline{T}_{\text{gas}}) + u(\eta)Pe\, v_n(\mathbf{x}_1)(H - \overline{H}_{\text{spray}}), \quad \mathbf{x}_1 \in \partial\Omega_1, \qquad (24)$$

where $v_n(\mathbf{x}_1)$ remains constant with η (since the surface geometry is steady), and is defined through $\overline{v}_{\mathbf{x}_P} = v_n(\mathbf{x}_1)u(\eta)$. In this form it is clear that the step change in $u(\eta)$ is in a sense equivalent to a change in *Pe* for the (pseudo) steady problem, *i.e.* (23) and (24) are parameterized solely by $u(\eta)$ *Pe*. Therefore, the billet-crown heat fluxes shown in Figures 13g and 13h should be approximately the same as the steady-state-crown heat flow which would be observed if the computations of Section 4.3 were repeated for $Pe = 1{\cdot}35$ and $Pe = 2{\cdot}25$, (*i.e.* in the intervals of fast billet growth). For $Pe = 1{\cdot}35$ the analogous (*i.e.* dimensional), billet surface growth is slower. The analogy is still correct, but the heat flow in Figure 13g has not had enough time to converge fully to the steady-state-crown heat flow for $\text{Pr} = 1{\cdot}35$. This is confirmed by lengthening the time interval between step jumps in $\dot{m}(\eta)$ and $u(\eta)$, in Figure 13i, and repeating the computation over a longer total time interval.

5. Conclusions

This paper has considered the problem of heat flow and solidification within an axisymmetric spray-formed billet, growing on a slow timescale. the problem consists of mathematically solving a nonlinear parabolic partial differential equation in two spatial dimensions, within an irregularly shaped expanding domain. A simple, but effective, computational algorithm for solving this problem has been developed, implemented and used to solve representative test problems.

In Section 4 the computational algorithm has been applied to the modelling of a number of realistic process situations. The main practical contributions of this paper are as follows.

1. If the billet-crown shape is kept steady and both $\dot{m}(\eta)$ and $u(\eta)$ are maintained steady, then a steady pattern of heat flow is likely to result (Section 4.2).
   (a) This is essential for the production of billets of consistent quality.
   (b) A smaller production Peclet number, *Pe* should result in a colder billet (all other parameters remaining fixed; Section 4.3).
2. It has been demonstrated clearly, by means of examples that significant transient heat flows can result from inadequately controlled billet growth.
   (a) If the start-up phase of the production run is not well controlled, the initial thermal transients, (see Sections 4.1.1 and 4.1.2), can persist for a significant proportion of the production run, (see Figures 8 and 9).
   (b) Maintenance of a steady crown shape alone is not sufficient to ensure that the heat flow is steady (Section 4.4).

The relative importance of the start-up phase to the steady-state phase clearly depends upon the length of billet being produced (equivalently, on η_{end}). Current billets are grown to lengths between 1 m and 2 m. Horizontal spray chambers, although presenting new engineering problem, allow the growth of much longer billets. The results in Section 4.4 strongly suggest that on-line "solidification control" of some form would be a practical necessity for such a process. Additionally, direct solution of (pseudo) steady-state crown heat-flow problems would appear to be sensible. This avoids both the problem of prescribing initial conditions and that of the moving billet surface. The main difficulty here is in fixing the lower limit of

the crown domain $z_1 = z^*$ and in prescribing a practically relevant boundary condition at $z_1 = z^*$.

Mathematical interest here is two-fold. Firstly, consideration of the slow-time equations (12)–(15), together with the boundary-layer equations of [19] as separate elements of an asymptotic approximation, is interesting. Secondly, as is illustrated well by the computational results, the boundary condition (13) which couples the growth of the expanding domain to the heat flow within the domain, can have a significant effect on the internal heat fluxes. Coupled growth and solidification are inherent in many materials processing applications as well as in other deposition/forming-type physical processes. It is felt that application-oriented studies (such as this one) would benefit from a rigorous mathematical study of the generic problem, which consists of a one-dimensional linear heat equation in an expanding interval, where the interval growth influences the heat flow through a boundary condition of the type (13). This is of course related to the Stefan problem.

Acknowledgements

This work was supported through a Teaching Company Associateship by Alcan International Ltd., Banbury, U.K. and the Oxford Centre for Advanced Materials and Composites, University of Oxford, (Grant Reference Number GR/F/12006). The author would like to express his thanks to Drs. Peter Alexander, Brian Cantor and Oliver Jacobs for their supervision during the course of this research.

The author also gratefully acknowledges financial support during the writing of this paper from the Austrian government, (Fonds zur Förderung der Wissenschaftlichen Forschung, project number P09647-PHY), and from the Christian Doppler Society.

Appendix

Table I. Alloy thermophysical parameters

$\hat{T}_s$	541°C	$\hat{K}_s$	151 W/m/°C
$\hat{T}_l$	631·8°C	$\hat{K}_l$	80 W/m/°C
$\hat{\rho}$	2400 kg/m^3	$\hat{c}$	1180 J/kg/°C
$\hat{L}$	317400 J/kg		

Notes

[1] The billet solidification timescale is usually found to be similar to that for billet growth, (see [19], Figure 3). This is not a coincidence. Billet growth rates are controlled so as not to exceed solidification rates. The billet rotates rapidly during formation ($\sim 10^2$ rpm), and so must be reasonably solid.

[2] Experimentally derived values for $\hat{h}_{\text{collector}}$ are in the range $\hat{h}_{\text{collector}} \approx 1000 - 5000\,\text{W/m}^2/\text{C}$ [9, 12]. Variation in the efficiency of thermal contact between different alloys and different process runs is quite likely. Values $\hat{h}_{\text{collector}} \sim 10^3\,\text{W/m}^2/\text{C}$ do indicate very effective heat transfer between collector and billet base; the exact value of $\hat{h}_{\text{collector}}$ will not be of much importance after a few seconds of billet growth. In strip spray-forming, a more precise value for $\hat{h}_{\text{collector}}$ would be required.

[3] Pyrometry is used during production, to give a measurement of average billet top surface temperature. Such measurements indicate that, during successful production runs, the average billet top surface temperature is close to the solidus temperature for many aluminum alloys. It is possible to enter the spray chamber after degassing, a few minutes after the end of the production run, and make direct measurements of the billet-surface temperature. In this way, an estimate of the temperature gradient existing down the length of the billet is made, (*e.g.* ≈ 100 C/m).

Billet growth rates are measured on-line [25] and reasonable estimates of $\overline{H}_{\text{spray}}$ are available (*e.g.* [11]). A combination of all this information shows that the conduction term in (13) is typically much less than the heat influx term on the top of the billet, where most of the spray is deposited. Therefore, (17) is likely to be approximately satisfied on the billet top surface (with $T \approx H \approx 0$). This generates the estimate for $\hat{h}_{\text{gas}}$.

Note that direct experimental measurement of $\hat{h}_{\text{gas}}$ or $\hat{T}_{\text{gas}}$) during production is nearly impossible. there is considerable turbulent mixing of the atomising gas in the spray chamber, due to high recirculatory gas velocities [8] and to rapid billet rotation. The spray chamber is sealed during production, allowing only non-intrusive measurement methods. It is extremely difficult to find reliable correlations for $\hat{h}_{\text{gas}}$, since the geometry range of validity of empirical correlations that are used for impinging jets in spray-cooling/drying applications, (*e.g.* [29]). Surface roughness and curvature complicate the use of simpler correlations, (*e.g.* flow over a flat plate), as does the 10 – 20% of the metal spray typically carried away in the gas stream.

[4] The value $\Delta r = \Delta z = 1/70$ has been arrived at after some numerical experimentation. For mesh sizes between $\Delta z = 1/30$ and $\Delta z = 1/100$ qualitative differences are only slight. Quantitative differences are largest closer to the billet collector boundary, rather than close to the growing surface of the billet. As described in Section 3.2.5, there will be an error associated with the prescription of initial conditions, which is dependent on the mesh size.

References

1. E.J. Lavernia and N.J. Grant, Spray deposition of metals; a review. *Mat. Sci. and Eng.* 98 (1988) 381–394.
2. A.G. Leatham, R.G. Brooks, J.S. Coombs and A.J.W. Ogilvy, The past, present and future of the Osprey preform process. Proceedings of *Int. Conf. on Spray Forming*, Swansea, U.K. (1990).
3. A.G. Leatham, J.S. Coombs, J.B. Forrest and S. Ahn, The Osprey process: an overview of the commercial developments for spray forming round billets in advanced ferrous and non-ferrous alloys, Proceedings of *2nd Pacific Rim Int. Conf. on Adv. Mat. and Processing*, Kyongju, Korea (1995).
4. B.P. Bewlay and B. Cantor, Modelling of spray deposition: measurements of particle size, gas velocity, particle velocity, and spray temperature in gas atomised sprays. *Met. Trans.* 21B (1990) 899–912.
5. G. Gillen, P. Mathur, D. Apelian and A. Lawley, Spray deposition: the interaction of material and process parameters. *Prog. in Powder Metall.* 42 (1986) 753–773.
6. P.S. Grant, B. Cantor, S. Rogers and L. Katgerman, A computer model for droplet and particle trajectories and thermal profiles in spray forming. *Cast Metals* 3 (1991) 227–773.
7. E.M. Gutierez, E.J. Lavernia, G.M. Trapaga, J. Szekely and N.J. Grant, A mathematical model of the spray deposition process. *Met. Trans.* 20A (1989) 71–85.
8. S. Rogers and L. Katgerman, Heat transfer and solidification of a stream of molten metal during atomisation by an impinging gas jet, Proceedings of the *5th Int. conf. on num. meth. in therm. probl.* Montreal (1987) 1806–1817.
9. S. Annavarapu, Spray casting of steel strip: Modelling and experimental studies. *Ph. D. thesis*, Drexel University (1989) 198 pp.
10. S. Annavarapu, D. Apelain and A. Lawley, Spray casting of steel strip: Process analysis. *Met. Trans.* 21A (1990) 3237–3255.
11. P.S. Grant, Spray forming of aluminium alloys. *D. Phil. thesis*, Oxford University (1991) 131 pp.
12. P. Mathur, Analysis of the spray deposition process. *Ph.D. thesis*, Drexel University (1988) 186 pp.
13. P. Mathur, S. Annavarapu, D. Apelian and A. Lawley, Spray casting: an integral model for process understanding and control. *Mat. Sci. and Eng.* A142 (1991) 261–276.
14. E.J. Lavernia, The evolution of microstructure during spray atomisation and deposition. *Int. J. of Rapid Solidif.* 5 (1989) 47–85.
15. X. Liang and E.J. Lavernia, Evolution of interaction domain microstructure during spray deposition. *Metallurg. and Mat. Trans. A* 25A (1994) 2341–2355.
16. H. Liu, E.J. Lavernia and R.H. Rangel, Numerical simulation of impingement of molten Ti, Ni and W droplets on a flat substrate. *J of Therm. Spray Techn.* 2 (1993) 369–378.
17. H. Liu, E.J. Lavernia and R.H. Rangel, Numerical investigation of micropore formation during substrate impact of molten droplets in plasma spray process. *Atomization and Sprays* 4 (1994) 369–384.
18. H. Liu, E.J. Lavernia and R.H. Rangel, Modeling of molten droplet impingement on a non-flat surface. *Acta Metall. Mater* 43 (1995) 2053–2072.
19. I.A. Frigaard, Solidification of aluminium spray-formed billets; an analysis of thin layering effects, *J. of Eng. Math.* 30 (1996) 417–443.
20. I.A. Frigaard, Mathematical modelling of an aluminium spray process. *D. Phil. thesis*, Oxford University (1993) 228 pp.
21. I.A. Frigaard, The dynamics of spray-formed billets. *SIAM J. Appl. Math.*, 55 (1995) 1161–1203.

22. I.A. Frigaard, Growth dynamics of spray-formed aluminium billets, Part 1; Steady state crown shapes. *J. Mat. Proc. Manufact. Sci*. 3 (1994) 173–193.
23. I.A. Frigaard, Growth dynamics of spray-formed aluminium billets, Part 2; Transient billet growth. *J. Mat. Proc. Manufact. Sci.* 3 (1995) 257–275.
24. I.A. Frigaard and O. Scherzer, Growing the perfect billet. *SIAM J. Appl. Math.*, accepted for publication March (1996).
25. J.J. Myerscough, On-line geometric control of a spray deposition process. *D. Phil. thesis*, Oxford University (1993) 207 pp.
26. A.A. Samarskii, On the convergence and accuracy of homogeneous difference schemes for one-dimensional and multidimensional parabolic equations. *U.S.S.R. J. Comp. Math. and Math. Phy.* 2 (1962) 654–696.
27. P.S. Grant and B. Cantor, Modelling of spray forming. *Cast Metals* 4 (1991) 140–151.
28. E.J. Lavernia, E.M. Gutierrez, J. Szekely and N.J. Grant, A mathematical model of the Liquid Dynamic Compaction process. Part 1: Heat flow in gas atomisation. *Int. J. of Rapid Solidif.* 4 (1988) 89–124.
29. H. Martin, Heat and mass transfer between impinging gas jets and solid surfaces. *Adv. in Heat and Mass Transf.* 13 (1977) Editors J.P. Hartnett and T.F. Irvine, Academic Press.